A Cubic B-Splines Approximation Method Combined with DWT and IBP for Single Image Super-resolution

Victor Kipkoech Mutai[1*]
Department of Electrical & Electronic Engineering
Dedan Kimathi University of Technology
Nyeri, Kenya

Elijah Mwangi[2]
Faculty of Engineering
University of Nairobi
Kenya

Ciira wa Maina[3]
Centre for Data Science and Artificial Intelligence
Dedan Kimathi University of Technology
Nyeri, Kenya

Abstract—The process of converting low-resolution images into high-resolution images by removing noise and estimating high-frequency information is known as image super-resolution. Aliased and decimated versions of the actual scenes are considered low-resolution images. The edges of high-resolution images produced by super-resolution from a single image are typically blurred. This paper proposes an approach to generate high-resolution image with sharp edges by combining a cubic B-Splines approximation, a discrete wavelet transform (DWT), and an iterative back-projection (IBP) edge-preserving weighted guided filter. A two-stage cubic B-Splines approximation, which includes pre-filtering and interpolation, is employed to up-sample the low-resolution image. The pre-filtering approach is used to transform pixel values to B-Splines coefficients. This approach minimizes blurring in the up-sampled image. The lost high-frequency information is then estimated using a one-level discrete wavelet transform based on the db1 wavelet. Finally, using a weighted guided filter, the resulting image is subjected to back-projection to obtain a high-resolution image. The proposed single-image super-resolution approach is applied on RGB colour images. The proposed method outperforms other selected approaches for comparison objectively in terms of PSNR and SSIM and also in visual quality.

Keywords—*Single-image super-resolution, pre-filtering, cubic B-Splines approximation, discrete wavelet transform (DWT), iterative back-projection (IBP), B-Splines coefficients*

I. INTRODUCTION

In many fields of digital imaging, there is usually a need for images of a higher resolution in a pre-processing stage for other subsequent operations. The main applications include diagnosis of medical conditions, pattern recognition, remote sensing, and surveillance [1]-[3]. The details that can be obtained from an image depends on its resolution. The capture of high-resolution images is not always feasible in surveillance systems because of limitations in terms of storage requirements, bandwidth for transmission of high-resolution images, power, and the cost of the image capturing device [4],[5]. Therefore, the image acquisition and transmission systems limit the resolution of the captured images, leading to constraints on the quality of the images available for interpretation and perception. As a result, image super-resolution (SR) is required to improve the information content in order to gain more details from the images. Multi-frame image reconstruction [6]-[8] and single-image super-resolution (SISR) [9]-[13] are the two types of super-resolution image reconstruction.

Image super-resolution aims at the recovery of the lost high-frequency information and preservation of the edges [14]. In this paper, an approach that combines cubic B-Splines approximation, discrete wavelet transform and iterative back-projection is proposed to achieve super-resolution from a single image. This is the first attempt to integrate the pre-filtering in cubic B-Splines approximation for image super-resolution. The key contributions of the proposed methodology over the current approaches are as follows:

(i). Design and integration of the pre-filtering to improve the up-scaling performance of the cubic B-Splines approximation.

(ii). Comparative analysis of wavelet image reconstruction to determine the best-performing wavelet among the three wavelet families (Daubechies, Symlets and Coiflets) in terms of the recovery of the lost frequency information.

(iii). Localization of the edges of the image using a weighted guided filter in back-projection to preserve and enhance details of the edges while avoiding widening of those edges.

(iv). Attaining good objective performance and visual quality with low computation time.

The rest of the paper is organized as follows. Section 2 presents the previous related works and contributions of this research paper. Section 3 presents the detailed proposed methodology. Experimental results and discussion are given in section 4. Summary of the findings and suggestions for further work are presented in section 5.

II. RELATED WORKS

Single-image super-resolution is an inverse optimization problem without a unique solution and thus very challenging because multiple solutions can be achieved based on the texture details. Direct interpolation using interpolation kernels [14], [15], wavelet transforms [16],[17], use of statistical approaches to estimate missing pixel values [18],[19], and example-based approaches [20], [21] are the sub-categories of single-image super-resolution. Bicubic interpolation is widely used in

up-scaling [22], [23]. However, it exhibits non-uniform gain which leads to distortions and larger lobes which introduces artifacts. The cubic B-Splines has been found to perform better than the widely used Keys' bicubic interpolation. However, it is an approximating function requiring a two-stage process [24]. Chen *et al.* [25] proposed an example-based approach that employs local multi-gradient level pattern prediction. The method results in high-quality output images compared to approaches selected for comparison. The approach is however limited by; (i) high computation requirements and (ii) high storage requirements for databases for training images.

The low-resolution (LR) image is used as the low-frequency sub-band, (LL), of the high-resolution image in the wavelet-based approach for super-resolution. The task is to estimate the high-frequency sub-bands in order to obtain a HR image. Demirel and Anbarjafari [26] proposed using a dual-tree complex wavelet transform (DT-CWT) for resolution enhancement of satellite images. They interpolated the input LR images using a bicubic interpolation function and the subsequent high-frequency sub-bands, and combined them to form a super-resolved image using the inverse DT-CWT. To improve image quality, Lidong *et al.* [27] combined the DWT and contrast limited adaptive histogram equalization (CLAHE) in their approach. The low-resolution mage is decomposed into 4 sub-bands. After that, the CLAHE is applied to the low-frequency sub-bands. Demirel and Anbarjafari [28] proposed an algorithm to improve image resolution using the DWT and SWT decompositions. To preserve the image's high-frequency information content, DWT based on the Daubechies 9/7 wavelet family is used. These approaches were however limited by (i) blurring in the highly textured areas and (ii) lack of comparison among the wavelets used in order to determine the wavelet that produce higher quality images.

In addition to estimating the high-frequency components, various methods have been employed to improve the super-resolved images quality further. Iterative back-projection [29]-[32] is one such process that minimizes the reconstruction error. Bareja and Modi [33] proposed a SISR based on IBP with an infinite symmetric exponential filter (ISEF) to preserve the edges. Ngocho and Mwangi [34] proposed back-projection using the Laplacian of Gaussian (LoG) kernel to enhance the edges and reduce noise in the resulting image. Makwana and Mehta [35] proposed an approach that combines IBP method with the Canny Edge detector and Gabor Filter for retrieval of the high-frequency information. They applied this method to grayscale images and compared them with existing algorithms. Despite the improvement in objective performance with these approaches, they employed global filters which leads to widening of the edges of the super-resolved images leading to reduced visual quality.

Motivations behind the proposed approach. In the previous works it was noted that despite the better performance of the cubic B-Splines than other interpolation kernels, direct interpolation using cubic B-Splines on the pixel values of an image leads to over-smoothing especially in the regions having high local variances [12],[13]. The proposed approach attempts

to rectify this issue by employing a pre-filter to compute the B-Splines coefficients which are then subjected to cubic B-Splines interpolation. In addition, various wavelets have been employed in estimation of the lost high-frequency information. However, no comparison among the wavelets used was tested. This investigation seeks to perform comparative analysis of various wavelet families to determine best performing wavelet in image-reconstruction [26]-[28]. Lastly, all the previous approaches employing iterative back-projection used global filters resulting in images with wider edges which is undesirable [31]-[35].

III. PROPOSED METHODOLOGY

The flowchart for the proposed single-image super-resolution approach is shown in Fig. 1. The proposed method combines a two-stage cubic B-Splines approximation, DWT, and iterative back-projection.

A. Cubic B-splines approximation

1) Pre-filtering

The pre-filtering step is used to compute the coefficients of an image using a direct B-splines filter. This method employs a recursively moving average filter to reduce the computational cost. The cubic B-Splines approximation is a two-stage process which begins with the estimation of the B-Splines coefficients, $c(k)$ from the pixel values of an image, $f(k)$. The challenge is to determine the coefficients such that the interpolation kernel passes through the pixel values exactly. The desired values $f(k)$ are obtained from the coefficients, $c(i)$ as in (1).

$$\sum_{i \in \mathbb{Z}} c(i)\beta^n(x-i)|_{x=k} = f(k) \qquad \forall k \in \mathbb{Z} \qquad (1)$$

Where n is the degree of B-Splines kernel.

Using discrete B-Splines kernel, (1) can be rewritten as in (2).

$$f(k) = b^n(k) * c(k) \qquad (2)$$

Where * is the convolution operator and $b^n(k) = \beta^n(x)|_{x=k}$. The B-Splines coefficients, $c(k)$ can be obtained as in (3)

$$c(k) = f(k) * \left(b^n(k)\right)^{-1} \qquad (3)$$

$\left(b^n(k)\right)^{-1}$ is the direct B-Splines filter. By sampling the discrete cubic B-splines interpolating kernel, (4) is obtained. The kernel is non-zero in the interval $-1 \le k \le 1$.

$$b^3(k) = \left(\frac{1}{6}, \frac{4}{6}, \frac{1}{6}\right) \qquad -1 \le k \le 1 \qquad (4)$$

By taking a z-transform of (4), (5) is obtained.

$$\beta^3(z) = \sum_{k=-1}^{1} b^3(k)z^{-k} = \frac{z+4+z^{-1}}{6} \qquad (5)$$

The direct cubic B-splines filter is obtained as in (6)-(9).

$$\left(b^3(k)\right)^{-1} \xleftarrow{\ z\ } \frac{1}{\beta^3(z)} \qquad (6)$$

$$\frac{1}{\beta^3(z)} = \frac{6}{z+4+z^{-1}} = 6\left(\frac{1}{1-\alpha z^{-1}}\right)\left(\frac{-\alpha}{1-\alpha z}\right)$$

$$= 6\left(\frac{-\alpha}{1-\alpha^2}\left(\frac{1}{1-\alpha z^{-1}} + \frac{1}{1-\alpha z} - 1\right)\right) \qquad (7)$$

$$6\left(\frac{-\alpha}{1-\alpha^2}\alpha^{|k|}\right) \xleftrightarrow{z} 6\left(\frac{-\alpha}{1-\alpha^2}\left(\frac{1}{1-\alpha z^{-1}} + \frac{1}{1-\alpha z} - 1\right)\right) \quad (8)$$

$$\left(b^3(k)\right)^{-1} = 6\left(\frac{-\alpha}{1-\alpha^2}\alpha^{|k|}\right) \qquad (9)$$
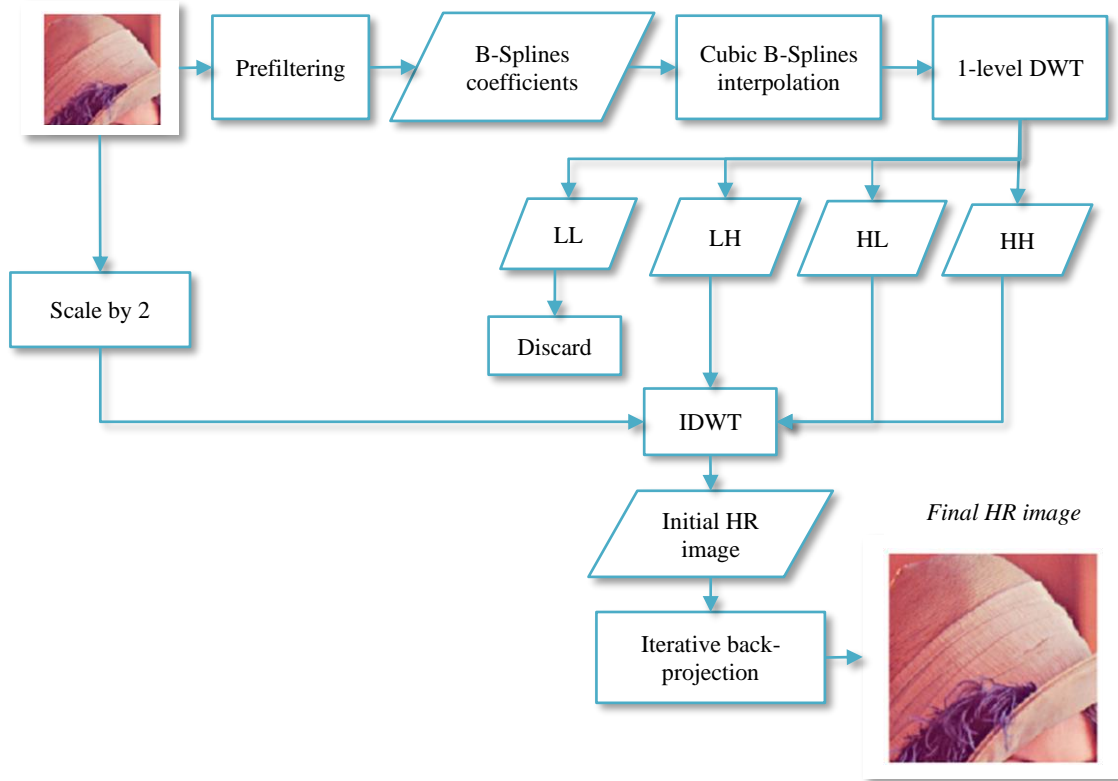
Where $\alpha = -2 + \sqrt{3}$.

Fig. 1:Proposed methodology

$(b^3(k))^{-1}$ is a direct cubic B-Splines filter having alternating sign change. The filter in (9) can be implemented using a causal filter in (10) and an anti-causal filter in (11). The cubic B-Splines coefficients are then obtained as in (12).

$$c^+(k) = f(k) + \alpha\, c^+(k-1) \qquad k = 1, \dots, J-1 \qquad (10)$$
$$c^-(k) = \alpha\big(c^-(k-1) - c^+(k)\big) \qquad k = J-2, \dots, 0 \qquad (11)$$
$$c(k) = \frac{c^-(k)}{6} \qquad (12)$$

$f(k)$ are the signal values, $c^+(k)$ is the causal filter, $c^-(k)$ is the anti-causal filter, J is the signal length, and $c(k)$ are the B-splines coefficients. The starting points for the two filters in (10) and (11) are given in (13) and (14) as follows.

$$c^+(0) = \sum_{k=0}^{k_0} f(k)\alpha^k \qquad (13)$$
$$c^-(J-1) = \frac{-\alpha}{1-\alpha^2}\big(c^+(J-1) + \alpha c^+(J-2)\big) \qquad (14)$$

2) Cubic B-Splines interpolation

The cubic B-Splines is based on the one-dimensional approximation kernel given in (15):

$$u(x) = \frac{1}{6}\begin{cases} 4 - 3|x|^2(2 - |x|) & 0 \le |x| < 1 \\ (2 - |x|)^3 & 1 \le |x| < 2 \\ 0 & 2 \le |x| \end{cases} \qquad (15)$$

This approximation kernel is applied in (16) to obtain new pixel values of the interpolated image, $f(x)$, from the B-splines coefficients, $c(k)$. Since the kernel is separable, for images, it is first applied along the rows and then along the columns sequentially.

$$f(x) = \sum_k c(k)u(x - k) \qquad (16)$$

The condition for the kernel to be interpolating is given in (17):

$$u(x) = \begin{cases} 1 & x = 0 \\ 0 & |x| = 1, 2, \dots \end{cases} \qquad (17)$$

It is noted that for cubic B-Splines, $u(0) \ne 1$ and hence does not satisfy the condition for being directly interpolating. Therefore, if it is applied directly to the pixel values of an image, it may lead to over-smoothing, especially in the regions with high local variances. This investigation seeks to determine whether pre-filtering will improve the performance of the cubic B-Splines approximation.

B. One-level Discrete Wavelet Transform

One level DWT is used to estimate the high-frequency sub-bands of the super-resolved image by passing the signal through a low-pass filter (LPF) and high-pass filter (HPF) [36]. It is used to decompose a signal to approximation and detail coefficients, each with half-the frequency components from the original signal. The decomposition is done in two stages for images, first along the rows and then along the image columns. The output of the operation is four sub-bands (*LL, LH, HL* and *HH*). This study will investigate which wavelet will produce higher quality super-resolution images better among the three wavelet families: Daubechies, Symlets and Coiflets.

C. Iterative Back-Projection (IBP)

Super-resolution is an inverse problem without a unique solution. A number of possible results can be limited by applying additional constraints leading to outputs closer to the ground truth images. The IBP is one such process to minimize the reconstruction error by projecting back the error difference, $e^{(n)}$ between the input LR image, and the low-resolution image from the resolution enhancement process, $SR^{(n)} \downarrow$. The process

is repeated until convergence is achieved. The IBP process can be summarized as in (18) and (19).

$$e^{(n)} = LR - SR^{(n)} \downarrow \qquad (18)$$

$$SR^{(n+1)} = SR^{(n)} + \left(e^{(n)} * p\right) \uparrow \qquad (19)$$

Where n denotes the nth iteration, $\uparrow$ is the up-sampling operator and $\downarrow$ is the down-sampling operator, p is the back-projection filter and $*$ is the convolution operator. In this paper, the weighted guided image filter [37],[38] has been selected as the back-projection filter. The weighted guided image filter combines the benefits of both the global and the local image filters. It incorporates edge-aware weighting that depends on whether the pixel values are on the edges or in smooth areas. Because of this weighting, the weighted guided filter maintains the sharpness of the edges of the image. Its complexity is also independent of the size of the kernel. Thus, we can use the larger kernel sizes can be employed with a negligible increase in computation times.

D. Proposed single image super-resolution process

The proposed image super-resolution process is given in steps (i) to (vii) as follows:

Step (i) The input LR image is subjected to a two-stage cubic B-Splines approximation with an up-sampling factors of 2 and 3. The LR image is subjected to a direct B-Splines filter (pre-filtering) in the first stage to transform the pixel values to coefficients in the B-Splines domain. In the second stage, the B-Splines coefficients are up sampled by integer factors of 2 and 3 using the cubic B-Splines approximation kernel.

Step (ii) The output image from the cubic B-Splines approximation is then decomposed into approximation coefficients (*LL*) and detail coefficients (*LH, HL* and *HH*) using one-level discrete wavelet transform based on the selected db1 wavelet.

Step (iii) The pixel values of the LR image are scaled by a factor of 2. The factor of 2 corresponds to the normalization factor for a one-level DWT. The scaled LR image and the detailed coefficients are subjected to one-level Inverse Discrete Wavelet Transform (IDWT) to get the initial HR image.

Step (iv) The initial HR image, $SR^{(0)}$ is down-sampled by a factor of 2 and 3 depending on the decimation factor used. The result is a low-resolution image, $LR^{(1)}$

$$LR^{(1)} = SR^{(0)} \downarrow \qquad (20)$$

Step (v) The low-resolution image, $LR^{(1)}$ is subtracted from LR to obtain an error image $e^{(1)}$

$$e^{(1)} = LR - LR^{(1)} \qquad (21)$$

Step (vi) The error image, $e^{(1)}$ is then convolved with a back-projection filter, $p,$ and up-sample it. The results are then added to the initial HR image.

$$SR^{(1)} = SR^{(0)} + \left(e^{(1)} * p\right) \uparrow \qquad (22)$$

Step (vii) Steps (iv) to (vi) are repeated until the convergence is achieved.

IV. RESULTS AND DISCUSSION

In this section, the experimental settings are first introduced, then performance of the proposed super-resolution algorithm and the comparison to other proposed approaches is reported.

A. Experimental settings

A total of 74 images were used in the super-resolution approach. The images are obtained from the public databases. The first set. The second image set contains the 24-bit RGB colour images from Signal and Processing Institute from University of California, Los Angeles, USA [41]. The dataset contains 36 high altitude aerial images of dimensions 512×512 and 1024×1024 pixels. The format is Tagged Image Format File (TIFF). The second set was obtained from Eastman Kodak Company [42]. It contains 24 RGB colour images of dimensions 512×768 pixels and 256×256 pixels. The last dataset was obtained from Deep AI [43]. It contains 14 images of dimensions 512×768 pixels commonly used for testing SR models. The test image sets contain images with significantly different frequency content and variations in texture and edges. The simulations were conducted in MATLAB R2020a environment. Fig. 2 illustrates a sample of 16 images from the databases.

For comparison, three single-image super-resolution methods have been used: LoG IBP [34], VDSR [39], NEDI [40], and bicubic interpolation as the baseline.

Fig.2: Sample test images from the selected databases. From the left to the right and top to the bottom: *Aerial1* (1024×1024), *Aerial2* (1024×1024), *Aerial3* (1024×1024), *Aerial4* (1024×1024) *Baby* (768×512), *Bird* (768×512), *Kodim03* (768×512), *Kodim10* (768×512), *Arctic hare* (256×256), *African girl* (768×512), *Lena* (512×512), *Monarch* (768×512), *peppers1*(512×512), *peppers2* (768×512) and *tulips* (768×512).

B. Experimental Results

The Peak Signal-to-Noise Ratio (PSNR) based on Mean Square Error (MSE) and Structural Similarity Index Measure (SSIM) are used to quantify the performance of the algorithm. The MSE measures the amount of lost frequency information in the image through pixel-by-pixel comparison. SSIM on the other hand considers effects of luminance and brightness of the image. The higher the PSNR and SSIM, the better the quality of the super-resolved image.

1) Investigation of the importance of pre-filtering in cubic B-Splines approximation

Two sets of experimental approaches were conducted to validate the effectiveness of the pre-filtering incorporated in cubic B-splines approximation. Grayscale version of the test images were used in this investigation. The test images were decimated by a factor of 2 to obtain LR images. In the first approach, the cubic B-splines interpolation was applied directly to the pixel values of the LR images. In the second approach, the proposed pre-filter was first used to transform the pixel values of the LR images to B-Splines coefficients. The cubic B-Splines interpolation was then applied to the B-Splines coefficients. Table I shows the results for the PSNR and SSIM comparison between the cubic B-Splines approximation which integrates the pre-filtering approach and direct interpolation using cubic B-Splines interpolation kernel. From Table I, the results indicates that cubic B-Splines approximation achieves better performance with the average PSNR and SSIM improvement of 3.43 dB and 0.05 respectively from direct interpolation. The other test images also gave similar results. These results indicates that applying a pre-filter to pixel values of an image before performing up-sampling with cubic B-Splines produces significantly better results than otherwise.

2) Comparative analysis for wavelet image reconstruction

The performance of the three wavelet families: Daubechies (db1, db2, db3 and db4), Coiflets (coif2, coif3 and coif4) and Symlets (sym2, sym3 and sym4) is evaluated in this subsection. The test images were converted to grayscale. They were then down-sampled followed by up-sampling by a factor of 2 using cubic B-Splines approximation. High-resolution images were then reconstructed based on the wavelets above. The results for a sample of ten images are shown in Table II. From the results obtained, the db1 wavelet achieves the best performance among the selected wavelets for all images. db1 wavelet has therefore been chosen in the proposed approach to estimate the missing frequency information in one-level DWT.

3) Convergence of the iterative back-projection (IBP)

In this subsection, the convergence of the IBP based on the weighted guided filter is analyzed. Fig. 3 indicates the PSNR values for the four selected test images versus the number of iterations. The convergence is achieved when the difference between the PSNR values for the consecutive iterations is less than 0.01dB. From Fig. 3, the PSNR values increase gradually with the number of iterations, and convergence is achieved within five steps. The other test images gave similar results.

TABLE I: COMPARISON BETWEEN CUBIC B-SPLINES APPROXIMATION (WITH PRE-FILTERING) AND DIRECT INTERPOLATION (WITHOUT PRE-FILTERING)

Image Labels ↓	PSNR (dB)			SSIM		
	Without Pre-filtering	*With Pre-filtering*	*Improvement*	*Without Pre-filtering*	*With Pre-filtering*	*Improvement*
Aerial1	29.39	30.66	1.28	0.72	0.77	0.05
Aerial5	31.41	33.99	2.58	0.74	0.79	0.05
Baby	32.21	35.26	3.05	0.90	0.95	0.04
Bird	30.19	34.39	4.11	0.92	0.97	0.05
Kodim03	30.20	32.59	2.39	0.87	0.91	0.04
Kodim10	29.02	30.82	1.80	0.84	0.89	0.05
Arctic hare	33.03	37.66	4.63	0.94	0.97	0.03
Lena	32.21	35.34	3.13	0.89	0.93	0.04
Peppers2	32.83	36.18	3.35	0.93	0.96	0.03
Tulips	29.50	33.52	3.26	0.86	0.92	0.06
AVERAGE	**30.99**	**34.42**	**3.43**	**0.85**	**0.90**	**0.05**

TABLE II: PSNR COMPARISON OF THE PERFORMANCE OF SELECTED WAVELETS IN IMAGE RECONSTRUCTION

| Image Labels ↓	Daubechies				Symlets			Coiflets		
	db1	*db2*	*db3*	*db4*	*sym2*	*sym3*	*sym4*	*coif2*	*coif3*	*coif4*
Aerial1	33.49	31.10	28.85	27.78	31.50	29.40	30.74	27.91	26.82	26.08
Aerial2	34.00	31.37	28.36	27.01	31.60	29.20	28.64	27.27	26.09	25.44
Aerial5	35.65	32.62	29.54	28.23	32.69	29.67	30.32	27.89	27.10	26.67
Baby	32.86	27.90	23.48	21.22	29.00	25.00	23.92	20.21	17.92	16.44
Bird	31.49	26.52	22.00	19.77	26.70	22.45	23.04	19.58	17.64	16.62
Kodim03	31.74	29.38	26.48	24.89	29.40	26.97	27.57	24.43	22.82	21.79
Arctic hare	35.10	28.95	24.11	21.73	29.70	24.15	26.13	21.33	19.14	17.98
Lena	31.21	27.41	23.20	21.03	28.00	23.56	24.66	21.12	18.97	17.75
Peppers2	34.28	30.96	26.54	24.05	31.40	26.89	27.04	24.27	21.58	19.93
Tulips	30.24	26.05	21.76	19.50	29.00	21.99	22.72	19.35	17.10	15.76
AVERAGE	**33.01**	**29.23**	**25.43**	**23.52**	**29.90**	**25.93**	**26.48**	**23.34**	**21.52**	**20.45**
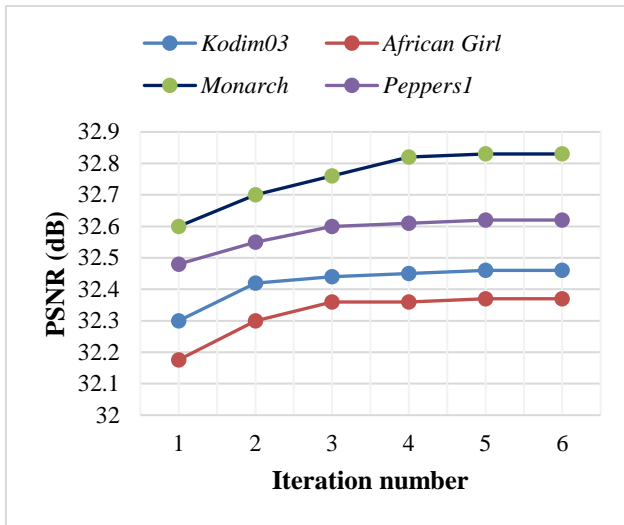
Fig. 3: PSNR variations against iterations for IBP

With the convergence achieved within five steps of IBP, the number of iterations in the proposed super-resolution approach was set to 5.

4) Comparison with recently proposed approaches

a) Objective performance

In this subsection, the proposed approach's SR performance in comparison with other approaches is analyzed on 16 test images from the specified databases, as shown in Fig. 3. The performance metrics used for this comparison are PSNR and SSIM. The objective performance results in terms of PSNR and SSIM with an upscaling factor of 2 are shown in Tables III and IV respectively. The proposed approach outperformed the selected approaches in 13 out of the 16 sample images.

In terms of SSIM, the proposed approach outperformed the selected approaches in all the selected images. The algorithm achieved highest average PSNR and SSIM. The best performance is highlighted in *red.*

For the high-altitude aerial images obtained from [41], the PSNR was found to differ by as much as 9 dB between the colour channels – *Aerial1* (Red=31.4 dB, Blue= 40.1 dB). This difference arises because the aerial images are almost one colour, with some colour channels containing very little information. The channel with low information returns very high PSNR values. In *aerial1* image, the red channel contains highest information followed by the green channel and lastly the blue channel.

The test image sets have images with significantly different frequency content and variations in texture and edges. The performance is therefore different for each image with images having high-frequency content achieving low PSNR and SSIM values when compared to images with low-frequency content. This is evident by *peppers1* (Red=31.8dB, Green=30.3dB and Blue=31.9dB) and *Arctic Hare* (Red=40.1dB, Green=42.3dB and Blue=43.1dB). *Arctic Hare* is a significantly smooth image thus low frequency content while *peppers1* image has high frequency content.

Interpolation approaches performs better in smooth images as observed in *Arctic Hare* where the proposed algorithm, LoG IBP [34], and Bicubic interpolation all achieved the highest SSIM of 0.98 for an up-scaling factor of 2 compared to the VDSR [39] algorithm, which gave 0.96.

The VDSR algorithm achieves better image quality in those images with patterns, for example, *Monarch*, where it achieved a PSNR improvement of over 0.9dB from the proposed algorithm in the blue and green colour channels.

TABLE III: Psnr Results With An Up-Sampling Factor Of 2

Image Labels	Proposed			VDSR [39]			Bicubic			LoG IBP [34]			NEDI [40]		
↓	R	G	B	R	G	B	R	G	B	R	G	B	R	G	B
Aerial1	31.4	34.6	40.1	31.0	34.4	39.3	30.5	33.7	39.2	30.4	33.6	38.9	29.5	33.0	38.9
Aerial2	33.1	36.1	39.9	32.4	35.7	38.3	32.0	35.1	39.0	32.5	35.4	38.8	29.5	33.3	38.2
Aerial5	34.7	35.1	35.5	34.3	34.9	35	33.6	34.1	34.6	33.6	34.0	34.2	32.5	33.4	34.7
Aerial8	29.9	33.8	41.3	29.5	33.6	40.1	29.0	32.9	40.4	29.0	32.8	40.2	28.2	32.1	39.8
Baby	36.5	36.6	36.5	34.9	35.1	34.9	35.4	35.6	35.5	36.0	36.2	36.0	31.6	32.0	32.3
Bird	36.2	36.5	36.3	34.8	35.2	34.3	34.7	35.1	34.8	36.2	36.5	36.1	29.7	30.2	30.0
Woman	31.8	31.8	31.9	32.4	32.4	32.4	30.6	30.7	30.7	31.5	31.6	31.7	27.2	27.2	27.3
Kodim03	33.7	33.5	33.4	34.0	33.9	33.6	32.6	32.5	32.6	33.0	32.9	32.7	31.2	31.2	31.7
Kodim10	32.0	31.9	31.8	32.7	32.7	32.5	31.1	31.0	31.0	31.5	31.5	31.3	29.1	28.8	29.1
Arctic hare	40.1	42.3	43.2	36.7	36.7	36.2	38.1	40.4	41.3	40.1	42.2	43.1	32.3	34.6	35.3
African girl	32.1	32.4	32.3	32.0	32.4	32.4	31.3	31.5	31.5	31.4	31.9	31.7	29.8	29.7	30.0
Lena	36.7	33.3	32.2	35.2	33.0	31.7	35.4	32.1	31.2	36.1	32.7	31.3	31.6	29.1	29.8
Monarch	33.0	32.7	32.6	33.6	33.6	33.5	31.8	31.6	31.5	32.7	32.4	32.3	28.6	28.4	28.6
Peppers1	31.8	30.3	31.9	31.0	30.2	31.0	30.4	29.0	30.9	30.4	29.4	31.0	29.5	27.0	29.4
Peppers2	37.8	37.5	37.2	36.6	37.2	35.5	36.5	36.3	36.1	37.5	37.2	36.7	32.2	32.5	32.7
Tulips	34.9	34.9	33.9	34.0	34.1	33.7	33.4	33	32.4	34.4	34.1	33.6	29.8	28.9	28.3
AVERAGE	34.5	34.6	35.6	33.5	33.8	34.6	32.9	33.4	34.5	33.5	33.7	35.0	30.1	30.7	32.3

TABLE IV: SSIM RESULTS WITH AN UP-SAMPLING FACTOR OF 2

Image Labels ↓	Proposed			VDSR [39]			Bicubic			LoG IBP [34]			NEDI [40]		
	R	G	B	R	G	B	R	G	B	R	G	B	R	G	B
Aerial1	0.84	0.88	0.92	0.78	0.85	0.90	0.77	0.83	0.91	0.77	0.83	0.91	0.74	0.82	0.90
Aerial2	0.89	0.89	0.92	0.86	0.88	0.90	0.85	0.87	0.9	0.87	0.88	0.9	0.76	0.81	0.88
Aerial5	0.89	0.89	0.88	0.80	0.81	0.78	0.80	0.81	0.78	0.79	0.79	0.76	0.76	0.77	0.77
Aerial8	0.85	0.89	0.95	0.83	0.88	0.94	0.82	0.86	0.94	0.83	0.87	0.94	0.78	0.84	0.93
Baby	0.96	0.96	0.95	0.95	0.95	0.93	0.95	0.95	0.93	0.96	0.95	0.94	0.91	0.91	0.89
Bird	0.98	0.98	0.96	0.97	0.96	0.93	0.97	0.97	0.95	0.98	0.98	0.96	0.92	0.92	0.91
Woman	0.95	0.96	0.96	0.95	0.95	0.95	0.94	0.95	0.94	0.95	0.95	0.95	0.90	0.91	0.90
Kodim03	0.95	0.93	0.92	0.93	0.93	0.92	0.91	0.92	0.9	0.92	0.92	0.91	0.89	0.89	0.88
Kodim10	0.94	0.95	0.91	0.92	0.92	0.92	0.90	0.90	0.89	0.90	0.91	0.90	0.86	0.86	0.86
Arctic hare	0.98	0.98	0.98	0.96	0.96	0.96	0.98	0.98	0.98	0.98	0.98	0.98	0.95	0.95	0.96
African girl	0.91	0.92	0.90	0.90	0.91	0.90	0.89	0.9	0.88	0.9	0.91	0.89	0.86	0.87	0.85
Lena	0.96	0.94	0.85	0.93	0.91	0.81	0.93	0.88	0.80	0.93	0.88	0.80	0.90	0.84	0.78
Monarch	0.96	0.96	0.95	0.96	0.95	0.95	0.96	0.95	0.94	0.96	0.96	0.95	0.93	0.93	0.92
Peppers1	0.85	0.88	0.85	0.79	0.86	0.82	0.78	0.84	0.82	0.78	0.84	0.82	0.78	0.83	0.8
Peppers2	0.97	0.97	0.95	0.96	0.97	0.93	0.96	0.97	0.94	0.96	0.97	0.94	0.94	0.94	0.91
Tulips	0.94	0.96	0.95	0.93	0.95	0.95	0.92	0.94	0.94	0.93	0.95	0.95	0.88	0.89	0.89
AVERAGE	0.93	0.94	0.93	0.90	0.92	0.91	0.88	0.89	0.89	0.90	0.91	0.91	0.86	0.87	0.88

For up-scaling factor of 3, the high-resolution images from the selected databases were decimated by a factor of 3 to obtain the low-resolution images. The images were then up-scaled by 3 using the proposed approach to obtain high-resolution images. The results were then compared to VDSR [39] and bicubic interpolation. LoG IBP [34] and NEDI [40] only up-scales the image by a factor of 2 and were therefore not compared for up-scaling factor of 3. Table V shows the PSNR and SSIM results for this comparison.

The approach with the best performance is highlighted in *red*. The selected approaches were applied independently to the three colour channels in RGB colour space in order to ensure the same treatment is applied in the colour images.

From Table V, the proposed approach outperforms the selected approaches in 15 out of the 16 test images from the sample. It also achieves highest SSIM for all the test images from the selected databases.

TABLE V: PSNR AND SSIM RESULTS FOR AN UP-SCALING FACTOR OF 3

Image Labels ↓	PSNR (dB)									SSIM								
	Proposed			VDSR [39]			Bicubic			Proposed			VDSR [39]			Bicubic		
	R	G	B	R	G	B	R	G	B	R	G	B	R	G	B	R	G	B
Aerial1	29.1	32.8	39.1	28.5	32.8	39.0	27.3	30.9	37.0	0.75	0.83	0.91	0.74	0.82	0.91	0.71	0.79	0.89
Aerial2	26.9	31.1	37.1	26.9	31.1	36.7	25.8	29.8	35.4	0.63	0.78	0.87	0.61	0.72	0.86	0.61	0.70	0.84
Aerial5	30.9	32.4	35.3	30.9	32.4	35.2	29.5	30.7	32.9	0.75	0.79	0.84	0.74	0.77	0.79	0.70	0.73	0.75
Aerial8	26.8	30.8	38.7	26.8	30.4	38.3	25.1	29.1	36.9	0.74	0.81	0.92	0.71	0.79	0.91	0.70	0.77	0.90
Baby	30.5	31.0	31.3	30.1	30.7	31.0	29.9	30.3	30.5	0.88	0.88	0.86	0.88	0.88	0.86	0.88	0.88	0.85
Bird	30.3	30.8	30.8	29.6	30.5	29.6	30.2	30.6	30.5	0.91	0.91	0.93	0.90	0.91	0.87	0.92	0.92	0.89
Woman	26.8	28.5	26.9	26.8	26.9	26.9	26.3	26.4	26.4	0.87	0.87	0.87	0.87	0.87	0.87	0.87	0.87	0.87
Kodim03	30.2	30.5	31.0	30.3	30.4	31.1	28.4	28.5	28.9	0.86	0.86	0.85	0.86	0.86	0.85	0.85	0.85	0.84
Kodim10	28.1	28.3	28.1	28.0	27.6	28.0	26.6	26.3	26.4	0.83	0.83	0.82	0.84	0.83	0.83	0.82	0.82	0.81
Arctic hare	29.5	32.2	33.3	29.3	31.6	32.5	29.1	31.8	33.0	0.91	0.92	0.95	0.90	0.91	0.91	0.90	0.91	0.90
African girl	28.2	28.4	28.6	28.1	28.8	28.1	27.1	27.3	27.3	0.82	0.86	0.85	0.82	0.84	0.81	0.81	0.82	0.81
Lena	30.6	28.3	29.7	30.2	28.2	29.7	30.1	27.6	28.3	0.89	0.83	0.81	0.87	0.82	0.77	0.87	0.81	0.75
Monarch	27.5	27.4	27.8	27.4	27.4	27.8	27.1	26.9	27.2	0.91	0.92	0.89	0.90	0.90	0.90	0.90	0.90	0.88
Peppers1	29.2	26.4	29.1	28.0	26.2	28.7	27.5	24.8	27.4	0.82	0.88	0.82	0.80	0.83	0.81	0.76	0.79	0.77
Peppers2	32.0	32.2	32.8	31.5	32.1	32.0	31.7	31.8	32.2	0.92	0.93	0.90	0.92	0.92	0.87	0.92	0.92	0.88
Tulips	28.9	28.2	27.5	29.0	28.2	27.3	28.4	27.8	27.2	0.84	0.85	0.84	0.85	0.85	0.84	0.82	0.82	0.82
AVERAGE	29.9	30.0	32.7	28.8	29.1	31.4	28.1	28.8	30.5	0.85	0.87	0.89	0.81	0.83	0.87	0.82	0.83	0.84

b) Visual quality comparison

Fig. 4 shows two images used for visual comparison. The blue rectangular box in the two selected images in shows the regions of interest to evaluate the performance of the super-resolution algorithms.
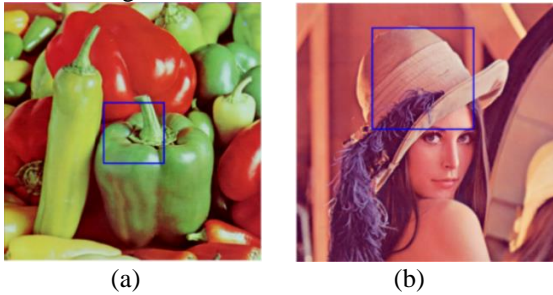

(a)   (b)

Fig. 4: Two test images used for visual comparison
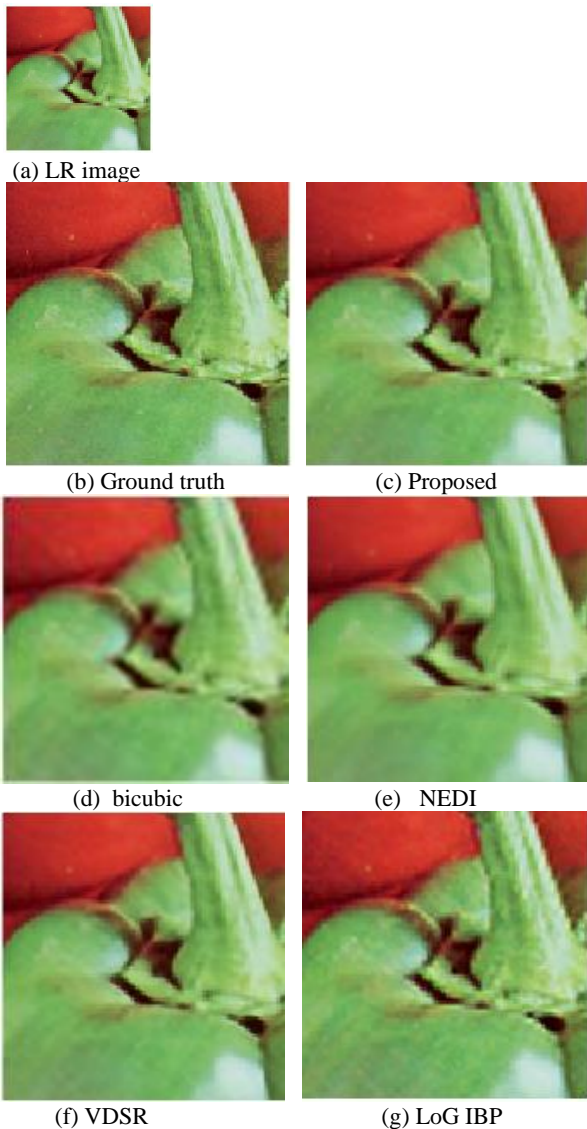(a) *Peppers1* image and (b) *Lena* image.

In terms of the visual comparison, Fig. 5 and Fig.6 shows the zoomed extracts obtained from *peppers1* and *Lena* image in Fig. 4 for the up-scaling factor of 2. From the zoomed extracts, the ground truth image has clear and sharper edges. The proposed method recovers the sharpness of the edges partially and maintains the natural texture of the images. The bicubic interpolation causes blurring of the output images NEDI, LoG IBP and VDSR maintains the edges but clearly smoothen out the highly textured areas. Other images also show similar results.
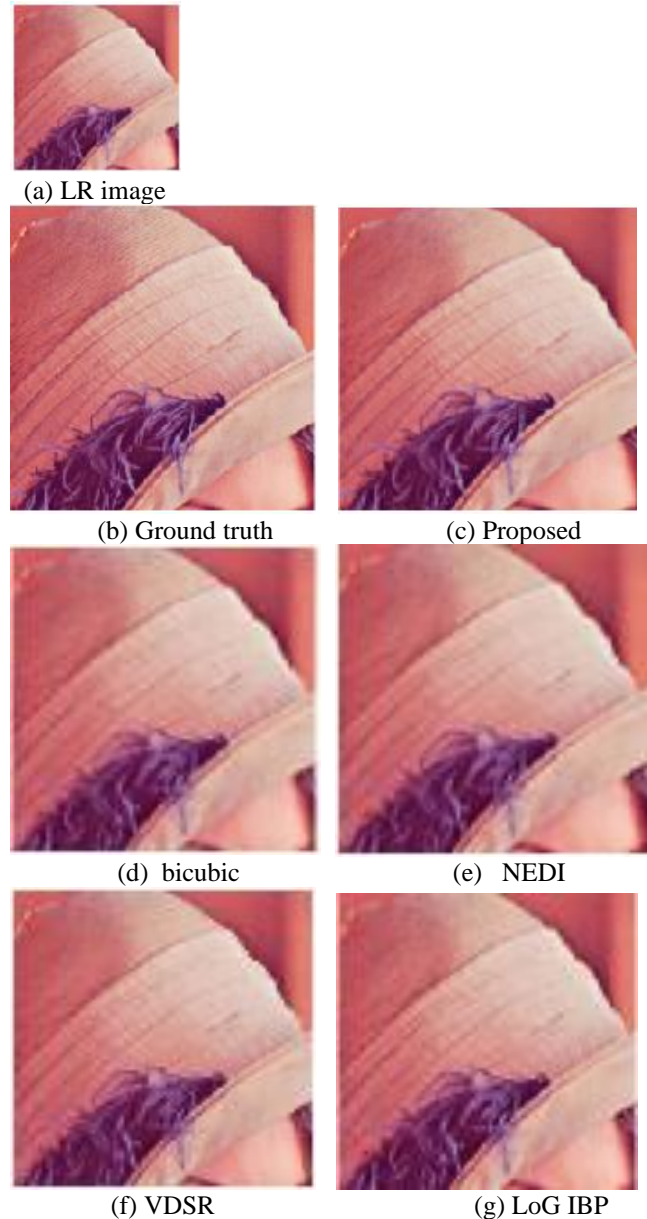

Fig. 5: Visual comparison for the zoomed extracts obtained from *Peppers1* image with an upscaling factor of 2

Fig. 6: Visual comparison for the zoomed extracts obtained from *Lena* image with an upscaling factor of 2

c) Computational complexity

To evaluate the computational complexity, a total of 10 images were used: *Aerial1, Aerial2, Aerial5, Aerial8, Kodim03, Kodim10, Lena, Monarch, Baby* and *Bird.* Despite this measure not being a scientific method of computing execution time, it however servs as an indicator of the computational complexity of each algorithm. The elapsed time it takes to super-resolve each image using the start and stop watch timers in MATLAB environment. Table VI and Table VII shows the results for the up-scaling factor of 2 and 3 respectively.

TABLE VI: EXECUTION TIME FOR UP-SCALING BY 2

Execution Time	METHOD				
	Bicubic	**Proposed**	**VDSR [39]**	**LoG IBP [34]**	**NEDI [40]**
Total time in seconds	6.21	16.18	238.21	20.61	982.1
Time per image in seconds	0.62	1.62	23.82	2.06	98.21

TABLE VII: EXECUTION TIME FOR UP-SCALING BY 3

Execution Time	METHOD		
	Proposed	**VDSR [39]**	**BICUBIC**
Total time in seconds	24.68	311.82	10.01
Time per image in seconds	2.47	31.18	1.00

From the results in Table VI and Table VII, it can be observed that: Bicubic interpolation has the shortest execution across the two up-scaling factors each taking less than 1 second to up-scale an image, The VDSR requires more than 20s per image and 4. The NEDI algorithm is computationally intensive requiring almost 100 seconds per image.

The proposed approach is second only to bicubic interpolation showing its computational efficiency with higher objective and visual performance.

V. CONCLUSION

This paper proposes a single image super-resolution approach that combines the cubic B-Splines approximation and discrete wavelet transform. The results demonstrated that the performance of the cubic B-splines can be significantly improved by first transforming the pixel values of an image to coefficients in the B-Splines domain before performing interpolation. The db1 wavelet was also found to recover the lost high-frequency information than other wavelets. In order to further enhance the sharpness of the edges of the super-resolved images a weighted guided filter has been added into the proposed approach as a back-projection filter. The proposed algorithm was tested on a set of 74 RGB colour images. The results for a sample of 16 images from the set have been reported for up-scaling factors of 2 and 3. The approach was applied independently to the three colour channels. It outperformed bicubic interpolation and the other selected super-resolution algorithms in visual quality.

The suggestions for further work are:

(i). Development of a 2-dimensional cubic B-Splines kernel. In this paper, a 1-dimensional kernel has been applied sequentially along the rows and the columns of the test images.

(ii). Up-scaling by a rational number e.g., 3/2. The up-scaling by integer factors of 2 and 3 were used in this paper.

(iii). Further work could also constitute improvement of the resolution of noisy images.

REFERENCES

[1]   L. Yue, H. Shen, J. Li, Q. Yuan, H. Zhang, and L. Zhang, "Image super-resolution: The techniques, applications, and future," *Signal Processing*, vol. 128, pp. 389–408, Nov. 2016, doi: 10.1016/j.sigpro.2016.05.002.

[2]   H. Wang, X. Gao, K. Zhang, and J. Li, "Single-Image Super-Resolution Using Active-Sampling Gaussian Process Regression," *IEEE Trans. on Image Process.*, vol. 25, no. 2, pp. 935–948, Feb. 2016, doi: 10.1109/TIP.2015.2512104.

[3]   Lizhe Wang, Ke Lu, and Peng Liu, "Compressed Sensing of a Remote Sensing Image Based on the Priors of the Reference Image," *IEEE Geosci. Remote Sensing Lett.*, vol. 12, no. 4, pp. 736–740, Apr. 2015, doi: 10.1109/LGRS.2014.2360457.

[4]   L. An and B. Bhanu, "Face image super-resolution using 2D CCA," *Signal Processing*, vol. 103, pp. 184–194, Oct. 2014, doi: 10.1016/j.sigpro.2013.10.004.

[5]   M.-C. Yang, C.-P. Wei, Y.-R. Yeh, and Y.-C. F. Wang, "Recognition at a long distance: Very low-resolution face recognition and hallucination," in *2015 International Conference on Biometrics (ICB)*, Phuket, Thailand, May 2015, pp. 237–242. doi: 10.1109/ICB.2015.7139090.

[6]   M. M. Khattab, A. M. Zeki, A. A. Alwan, A. S. Badawy, and L. S. Thota, "Multi-Frame Super-Resolution: A Survey," in *2018 IEEE International Conference on Computational Intelligence and Computing Research (ICCIC)*, Madurai, India, Dec. 2018, pp. 1–8. doi: 10.1109/ICCIC.2018.8782382.

[7]   N. L. Nguyen, J. Anger, A. Davy, P. Arias, and G. Facciolo, "Self-supervised multi-image super-resolution for push-frame satellite images," in *2021 IEEE/CVF Conference on Computer Vision and Pattern Recognition Workshops (CVPRW)*, Nashville, TN, USA, Jun. 2021, pp. 1121–1131. doi: 10.1109/CVPRW53098.2021.00123.

[8]   J. I. Delgado-Centeno, P. J. Sanchez-Cuevas, C. Martinez, and M. A. Olivares-Mendez, "Enhancing Lunar Reconnaissance Orbiter Images via Multi-Frame Super Resolution for Future Robotic Space Missions," *IEEE Robot. Autom. Lett.*, vol. 6, no. 4, pp. 7721–7727, Oct. 2021, doi: 10.1109/LRA.2021.3097510.

[9]   Y. Zhang, Q. Fan, F. Bao, Y. Liu and C. Zhang, "Single-Image Super-Resolution Based on Rational Fractal Interpolation," in *IEEE Transactions on Image Processing*, vol. 27, no. 8, pp. 3782-3797, Aug. 2018, doi: 10.1109/TIP.2018.2826139.

[10]   H. Kim and G. Kim, "Single Image Super-Resolution Using Fire Modules With Asymmetric Configuration," *IEEE Signal Process. Lett.*, vol. 27, pp. 516–519, 2020, doi: 10.1109/LSP.2020.2980172.

[11]   Y. Yan, W. Ren, X. Hu, K. Li, H. Shen, and X. Cao, "SRGAT: Single Image Super-Resolution With Graph Attention Network," *IEEE Trans. on Image Process.*, vol. 30, pp. 4905–4918, 2021, doi: 10.1109/TIP.2021.3077135.

[12]   T. Briand and P. Monasse, "Theory and Practice of Image B-Spline Interpolation," *Image Processing On Line*, vol. 8, pp. 99–141, Jul. 2018, doi: 10.5201/ipol.2018.221.

[13]   F. Champagnat and Y. Le Sant, "Efficient Cubic B-spline Image Interpolation on a GPU," *Journal of Graphics Tools*, vol. 16, no. 4, pp. 218–232, Oct. 2012, doi: 10.1080/2165347X.2013.824736.

[14]   R. Lan *et al.*, "Cascading and Enhanced Residual Networks for Accurate Single-Image Super-Resolution," *IEEE Trans. Cybern.*, vol. 51, no. 1, pp. 115–125, Jan. 2021, doi: 10.1109/TCYB.2019.2952710.

[15] Y. Li, F. Qi, and Y. Wan, "Improvements On Bicubic Image Interpolation," in *2019 IEEE 4th Advanced Information Technology, Electronic and Automation Control Conference (IAEAC)*, Chengdu, China, Dec. 2019, pp. 1316–1320. doi: 10.1109/IAEAC47372.2019.8997600.

[16] P. Megha, M. Swarna, V. Sowmya, and K. P. Soman, "Low contrast satellite image restoration based on adaptive histogram equalization and discrete wavelet transform," in *2016 International Conference on Communication and Signal Processing (ICCSP)*, Melmaruvathur, Tamilnadu, India, Apr. 2016, pp. 0402–0406. doi: 10.1109/ICCSP.2016.7754166.

[17] T. D. Gadhiya, A. K. Roy, S. K. Mitra, and V. Mall, "Use of discrete wavelet transform method for detection and localization of tampering in a digital medical image," in *2017 IEEE Region 10 Symposium (TENSYMP)*, Cochin, India, Jul. 2017, pp. 1–5. doi: 10.1109/TENCONSpring.2017.8070082.

[18] X.-L. Tian and J.-Q. Chen, "A Fast Algorithm for Single Image Super-Resolution Reconstruction via Revised Statistical Prediction Model," in *2016 International Conference on Information System and Artificial Intelligence (ISAI)*, Hong Kong, China, Jun. 2016, pp. 305–309. doi: 10.1109/ISAI.2016.0071.

[19] T. Peleg and M. Elad, "A Statistical Prediction Model Based on Sparse Representations for Single Image Super-Resolution," *IEEE Trans. on Image Process.*, vol. 23, no. 6, pp. 2569–2582, Jun. 2014, doi: 10.1109/TIP.2014.2305844.

[20] K.-W. Hung, Z. Zhang, and J. Jiang, "Real-Time Image Super-Resolution Using Recursive Depthwise Separable Convolution Network," *IEEE Access*, vol. 7, pp. 99804–99816, 2019, doi: 10.1109/ACCESS.2019.2929223.

[21] T. Lu, Y. Wang, J. Wang, W. Liu, and Y. Zhang, "Single Image Super-Resolution via Multi-Scale Information Polymerization Network," *IEEE Signal Process. Lett.*, vol. 28, pp. 1305–1309, 2021, doi: 10.1109/LSP.2021.3084522.

[22] R. Li and Q. Lv, "Image sharpening algorithm based on a variety of interpolation methods," in *2012 International Conference on Image Analysis and Signal Processing*, Huangzhou, China, Nov. 2012, pp. 1–4. doi: 10.1109/IASP.2012.6425043.

[23] W. Zhang, K. Jiang, L. Wang *et al.*, "A Wavelet-Based Asymmetric Convolution Network for Single Image Super-Resolution," *IEEE Access*, vol. 9, pp. 28976–28986, 2021, doi: 10.1109/access.2021.3058648.

[24] P. Thevenaz, "Image Interpolation and Resampling," in *Handbook of Medical Image Processing and Analysis*, Elsevier, 2009, pp. 465–493. doi: 10.1016/B978-012373904-9.50037-4.

[25] C.-W. Chen, F.-K. Hsu, D.-W. Yang, J. Wang, and M.-D. Shieh, "Effective model construction for enhanced prediction in example-based super-resolution," in *2016 IEEE Asia Pacific Conference on Circuits and Systems (APCCAS)*, Jeju, South Korea, Oct. 2016, pp. 156–159. doi: 10.1109/APCCAS.2016.7803921.

[26] H. Demirel and G. Anbarjafari, "Satellite Image Resolution Enhancement Using Complex Wavelet Transform," *IEEE Geosci. Remote Sensing Lett.*, vol. 7, no. 1, pp. 123–126, Jan. 2010, doi: 10.1109/LGRS.2009.2028440.

[27] H. Lidong, Z. Wei, W. Jun, and S. Zebin, "Combination of contrast limited adaptive histogram equalisation and discrete wavelet transform for image enhancement," *IET Image Processing*, vol. 9, no. 10, pp. 908–915, Oct. 2015, doi: 10.1049/iet-ipr.2015.0150.

[28] H. Demirel and G. Anbarjafari, "Image Resolution Enhancement by Using Discrete and Stationary Wavelet Decomposition," *IEEE Trans. on Image Process.*, vol. 20, no. 5, pp. 1458–1460, May 2011, doi: 10.1109/TIP.2010.2087767.

[29] S. Lei, X. Liao, and Z. Tao, "Content-aware Up-sampling for Single Image Super-resolution," in *2020 Asia-Pacific Conference on Image Processing, Electronics and Computers (IPEC)*, Dalian, China, Apr. 2020, pp. 213–217. doi: 10.1109/IPEC49694.2020.9115143.

[30] F. Deeba, S. Kun, F. Ali Dharejo, and Y. Zhou, "Wavelet-Based Enhanced Medical Image Super Resolution," *IEEE Access*, vol. 8, pp. 37035–37044, 2020, doi: 10.1109/access.2020.2974278.

[31] E. Castro, M. Nakano, G. Sanchez, and H. Perez, "Improvement of Image Super-resolution Algorithms using Iterative Back Projection," *IEEE Latin Am. Trans.*, vol. 15, no. 11, pp. 2214–2219, Nov. 2017, doi: 10.1109/TLA.2017.8070429.

[32] J.-S. Yoo and J.-O. Kim, "Noise-Robust Iterative Back-Projection," *IEEE Trans. on Image Process.*, vol. 29, pp. 1219–1232, 2020, doi: 10.1109/TIP.2019.2940414.

[33] M. N. Bareja and C. K. Modi, "An Improved Iterative Back Projection Based Single Image Super Resolution Approach," *Int. J. Image Grap.*, vol. 14, no. 04, p. 1450015, Oct. 2014, doi: 10.1142/S0219467814500156.

[34] B. M. Ngocho and E. Mwangi, "Single image super resolution with guided back-projection and LoG sharpening," in *2016 18th Mediterranean Electrotechnical Conference (MELECON)*, Lemesos, Cyprus, Apr. 2016, pp. 1–6. doi: 10.1109/MELCON.2016.7495419.

[35] R. R. Makwana and N. Mehta, "Single Image Super-Resolution VIA Iterative Back Projection Based Canny Edge Detection and a Gabor Filter Prior," *undefined*, 2013, Accessed: Dec. 21, 2021. [Online]. Available: https://www.semanticscholar.org/paper/Single-Image-Super-Resolution-VIA-Iterative-Back-a-Makwana-Mehta/3fab67d595249b485bf3e0b76e7749ff68695c45

[36] Cé. Vonesch, T. Blu, and M. Unser, "Generalized Daubechies Wavelet Families," *IEEE Trans. Signal Process.*, vol. 55, no. 9, pp. 4415–4429, Sep. 2007, doi: 10.1109/TSP.2007.896255.

[37] Z. Li, J. Zheng, Z. Zhu, W. Yao, and S. Wu, "Weighted Guided Image Filtering," *IEEE Transactions on Image Processing*, vol. 24, no. 1, pp. 120–129, Jan. 2015, doi: 10.1109/TIP.2014.2371234.

[38] H. Geethu, S. Shamna, and J. J. Kizhakkethottam, "Weighted Guided Image Filtering and Haze Removal in Single Image," *Procedia Technology*, vol. 24, pp. 1475–1482, 2016, doi: 10.1016/j.protcy.2016.05.248.

[39] J. Kim, J. K. Lee, and K. M. Lee, "Accurate Image Super-Resolution Using Very Deep Convolutional Networks," in *2016 IEEE Conference on Computer Vision and Pattern Recognition (CVPR)*, Las Vegas, NV, USA, Jun. 2016, pp. 1646–1654. doi: 10.1109/CVPR.2016.182.

[40] Xin Li and M. T. Orchard, "New edge-directed interpolation," *IEEE Trans. on Image Process.*, vol. 10, no. 10, pp. 1521–1527, Oct. 2001, doi: 10.1109/83.951537.

[41] "Test Images." https://homepages.cae.wisc.edu/~ece533/images/ (accessed Oct. 15, 2020).

[42] R. Franzen, "Kodak Lossless True Color Image Suite", Eastman Kodak, 27 January 2020. [Online]. Available: http:\\r0k.us/graphics/kodak/. (accessed Feb. 06, 2022).

[43] "Set14 Super Resolution Dataset'," DeepAI. https://deepai.org/dataset/set14-super-resolution (accessed Feb. 06, 2022).